THE JOURNAL OF PHYSICAL CHEMISTRY A

Article

pubs.acs.org/JPCA

Photoelectron Spectroscopy of *cis*-Nitrous Acid Anion (*cis*-HONO$^-$)

Allan M. Oliveira,[†] Julia H. Lehman,[†] Anne B. McCoy,*[,‡] and W. Carl Lineberger*[,†]

[†]JILA, and Department of Chemistry and Biochemistry, University of Colorado, Boulder, Colorado 80309, United States

[‡]Department of Chemistry, University of Washington, Seattle, Washington 98195, United States

Supporting Information

ABSTRACT: We report photoelectron spectra of *cis*-HONO$^-$ formed from an association reaction of OH$^-$ and NO in a pulsed, plasma-entrainment ion source. The experimental data are assigned to the *cis*-HONO$^-$ isomer, which is predicted to be the global minimum on the anion potential energy surface. We do not find evidence for a significant contribution from *trans*-HONO$^-$. Electron photodetachment of *cis*-HONO$^-$ with 1613, 1064, 532, 355, and 301 nm photons accesses the ground $\tilde{X}$ ^{1}A′ (S_0) and excited $\tilde{a}$ ^{3}A″ (T_1) states of neutral HONO. The photoelectron spectrum resulting from detachment forming *cis*-HONO (S_0) exhibits a long vibrational progression, dominated by overtones and combination bands involving the central O−N stretching and ONO bending vibrations. This indicates that there is a significant change in the central O−N bond length between *cis*-HONO$^-$ and *cis*-HONO (S_0). The electron affinity (EA) of *cis*-HONO is determined to be 0.356(8) eV. We also report the dissociation energy (D_0) of *cis*-HONO$^-$, forming OH$^-$ + NO, as 0.594(9) eV, which is a factor of 4 decrease in the central O−N bond strength compared to neutral *cis*-HONO. The T_1 state of *cis*-HONO is shown to be ∼2.3 eV higher in energy than *cis*-HONO (S_0). Electron photodetachment to form *cis*-HONO (T_1) accesses a transition state along the HO−NO bond dissociation coordinate. The resulting photoelectron spectrum exhibits broad peaks spaced by the terminal N═O stretching frequency. Electronic structure calculations and photoelectron spectrum simulations reported here show very good agreement with the experimental data.

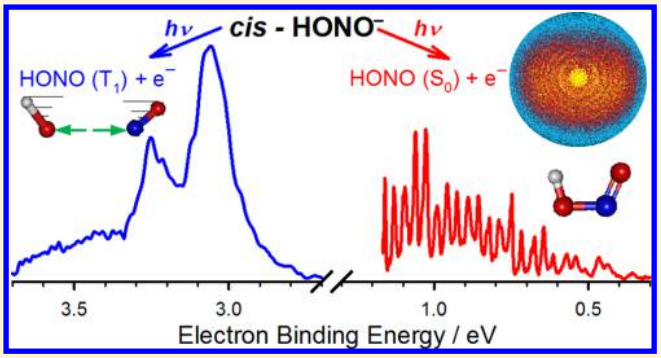

I. INTRODUCTION

Nitrous acid (HONO) is an important atmospheric source of OH radicals.[1−3] HONO is predicted to be formed at night by heterogeneous conversion[2] and disproportionation[4] of nitrogen dioxide (NO_2) through reactions with water or hydrocarbons, as well as by direct emissions in polluted urban areas.[2] The central O−N bond is broken following irradiation by sunlight between 300 and 400 nm, giving rise to OH radicals in the atmosphere.[5] Because of its atmospheric importance, HONO has been the subject of many investigations, both theoretical[6−8] and experimental.[9−20] Microwave[18,21] and Fourier transform infrared spectroscopic studies[13,14] of HONO in its ground electronic state determined the structure, rotational constants, and six fundamental frequencies of both *cis* and *trans* isomers. In addition, the weakest bond in HONO was determined to be the central O−N bond, with a ground state bond dissociation energy of 2.079 eV for the lower energy *trans* isomer.[16,22]

The electronic states of HONO have also been investigated, with experimental studies using photon energies spanning UV to deep UV wavelengths to access high-lying electronic states, giving rise to the production of either OH + NO or H + NO_2 in the atmosphere. By use of UV absorption spectroscopy, the $\tilde{A}$ ^{1}A″ (S_1) state of *cis*-HONO was observed to be 3.26 eV higher in energy than the $\tilde{X}$ ^{1}A′ (S_0) ground state.[23,24] Vertical excitation from the ground electronic state to the S_1 surface, which is repulsive along the HO−NO bond dissociation coordinate, results in breaking of the central O−N bond. This is likely to be the atmospheric pathway for OH radical formation.[25] Yu et al.[7] performed complete active space (CAS) calculations on the *trans* isomer of HONO, investigating the four lowest energy singlet and triplet excited electronic states and their stabilities with respect to the HO−NO bond dissociation. The lowest energy excited state, the $\tilde{a}$ ^{3}A″ (T_1) state, was calculated to be approximately 2.3 eV higher in energy than the S_0 ground state and dissociates to OH + NO but with a small (0.19 eV) barrier along the dissociation coordinate.[7] While this electronic state is energetically accessible with visible light irradiation, spin selection rules prevent observation of the T_1 state by direct absorption methods.[8] The T_1 state can be accessed, however, via an intersystem crossing transition from the excited $\tilde{B}$ ^{1}A′ (S_2) state of HONO.[7,26,27] Thus, experimental studies on the T_1 state would be useful in understanding how this electronic state contributes to atmospheric OH production.

Received: December 2, 2015
Revised: February 14, 2016
Published: February 17, 2016

DOI: 10.1021/acs.jpca.5b11797
J. Phys. Chem. A 2016, 120, 1652−1660

Beyond studying the electronic structure of HONO, there has also been interest in the proposed mechanisms for HONO formation in the atmosphere.[1] In addition to the previously mentioned pathways, an alternative proposed mechanism for HONO generation is through its negative ion.[17] Negative-ion chemistry of molecules containing H, O, and N is relevant in the atmosphere.[28] The hydroxide anion (OH^-) is known to be formed through hydrogen atom abstraction from hydrocarbons by O^-.[28] Van Doren et al.[17] have explored the associative detachment reaction: $OH^- + NO \rightarrow HONO + e^-$. The associative detachment process is believed to arise primarily from autodetachment from $HONO^-$ vibrational continuum states, making it an inefficient process compared to dissociation back to reactants.[17] However, no experimental data are available for either the dissociation of $HONO^-$ to OH^- + NO or the electron affinity (EA) of HONO. Calculations predict this anion's dissociation energy to be 0.49 eV [17] or 0.86 eV,[8] with a predicted EA(HONO) of either 0.15 eV [17] or 0.66 eV,[8] depending on the level of theory employed. Experimental data on $HONO^-$ are necessary before a conclusion can be drawn concerning the importance of the anion in the atmosphere or its possible role in the production of neutral HONO.

In this work, we report photoelectron spectra of *cis*-$HONO^-$, yielding spectroscopic information on *cis*-HONO (S_0), EA(*cis*-HONO), and the dissociation energy of *cis*-$HONO^-$ to form OH^- + NO. Electron detachment from *cis*-$HONO^-$ using higher photon energies produces *cis*-HONO (T_1) in a configuration near a transition state along the central O−N bond dissociation coordinate. Possible contributions from higher excited states of *cis*-HONO and contributions from the *trans*-isomer are also considered and are found to provide at most small contributions to the measured signal. Quantum-chemical calculations provide additional insights into the resulting photoelectron spectrum.

II. METHODS

II.A. Experimental Methods. We employ a velocity map imaging (VMI) anion photoelectron spectrometer, described in detail previously.[29] In brief, we produce $HONO^-$ by reacting hydroxide (OH^-) with nitric oxide (NO) in a pulsed plasma entrainment anion source.[30] This anion source consists of two perpendicular pulsed General Valves: the primary supersonic expansion (40 psig, 0.5% NO in argon) and an effusive flow (55 psig, 1% O_2, 30% H_2, and the balance Ar). The low-flow side valve generates ions in a pulsed electrical discharge (−2000 V, 40−100 μs); the generated plasma is then entrained into the main supersonic gas expansion. An additional purification procedure was used to remove NO_2 from the NO mixture and is described in the Supporting Information. The small amount of NO in the main gas expansion reacts with the OH^- generated in the plasma, forming $HONO^-$, while the argon buffer gas provides collisional cooling. The anion source that is used in this study exhibits a remarkable capability to produce anions from ion−molecule association reactions and the ability to cool the newly formed anions to their vibrational ground state.[30]

Approximately 25 cm downstream from the main expansion, the negative ions are extracted into a Wiley−McLaren time-of-flight (TOF) mass spectrometer where they are steered, separated by their mass-to-charge ratio (m/z), and spatially focused onto an inline microchannel plate (MCP) detector. Prior to the inline MCP, an appropriately timed laser pulse intersects the ions with the desired m/z ratio in the interaction region, generating a small packet of photodetached electrons in the first stage of the VMI photoelectron spectrometer. The 3D velocity distribution of the photodetached electrons is velocity-mapped onto a 2D MCP/phosphor screen position-sensitive detector coupled to a CCD camera. The resulting photoelectron image is converted into a photoelectron spectrum, first as a function of velocity by applying an inverse Abel transformation using the BASEX algorithm[31] and then as a function of kinetic energy by applying a Jacobian transformation.

The spectral resolution of the VMI spectrometer improves as the electron kinetic energy decreases. Therefore, we use different photon energies to obtain well-resolved photoelectron spectra of *cis*-$HONO^-$ over the full spectral range of interest. Two electronic states of neutral *cis*-HONO are identified in this study. To obtain the full photoelectron spectrum accessing the lowest state, *cis*-HONO (S_0), we utilize the second harmonic of a Nd:YAG laser (532 nm). For higher resolution ground state spectra, we employ 1064 nm (Nd:YAG fundamental) and 1613 nm radiation (difference frequency mixing of 1064 nm and dye-laser generated 640 nm radiation). The T_1 state of *cis*-HONO is investigated using both the third harmonic of the Nd:YAG laser (355 nm) and 301 nm photons from frequency-doubling the dye-laser generated 602 nm radiation.

In this paper, we report photoelectron spectra as functions of the electron binding energy (eBE = $h\nu$ − eKE), a quantity that is independent of the laser wavelength used for photodetachment. The energy scale in the photoelectron spectra accessing *cis*-HONO (S_0) is calibrated using the O_2^- photoelectron spectrum.[32] To calibrate the photoelectron spectra of detachment to form *cis*-HONO (T_1), we use the photoelectron spectrum of I^-.[33] The experimental resolution, characterized by the full width at half-maximum (fwhm) of a peak divided by its electron kinetic energy (fwhm/eKE), is approximately 3% for an electron kinetic energy of ∼0.5 eV. The reported spectra contain data points much more closely spaced than this resolution and are appropriately smoothed to reflect this.

II.B. Theoretical Methods. In this work, all electronic structure calculations were performed using the Gaussian 09 software package.[34] One-dimensional cuts through the potential energy surfaces (CBS-QB3 composite method) as functions of the central O−N bond distance (labeled as $r_{ON,c}$ for the remainder of this manuscript) with all other coordinates optimized are plotted in Figure 1. As is seen, in cases of electron photodetachment to form the S_0 state of *cis*-HONO, the shift in the equilibrium value of $r_{ON,c}$ between the anion surface (plotted in green) and the S_0 surface for *cis*-HONO (plotted in black) leads us to expect that there will be evidence of a vibrational progression in at least the central O−N stretching mode in the photoelectron spectrum. In contrast, the T_1 state of *cis*-HONO at the anion equilibrium geometry is near a transition state along the HO−NO bond dissociation coordinate. In this case, a broad, unresolved photoelectron spectrum is expected. The difference in the nature of the potential surfaces in the vertical detachment region for the S_0 (bound) and T_1 (dissociative) states of *cis*-HONO requires different approaches to model the photoelectron spectra.

To aid the interpretation of the photoelectron spectrum following electron detachment to form *cis*-HONO (S_0), ab initio calculations for both *cis*-$HONO^-$ and *cis*-HONO (S_0) were performed at the MP2/aug-cc-pVTZ (UMP2 for the anion) and CCSD(T)/aug-cc-pVTZ levels of theory/basis-set for geometry optimization and relative energies. This choice of

DOI: 10.1021/acs.jpca.5b11797
J. Phys. Chem. A 2016, 120, 1652−1660

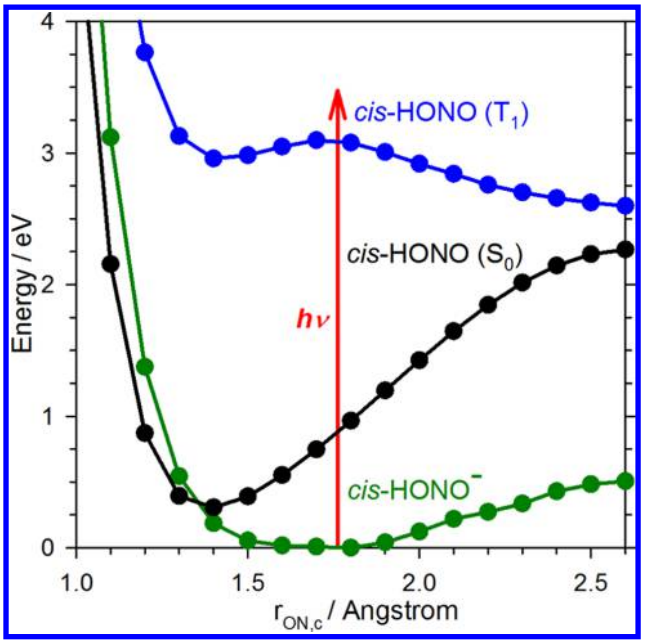

Figure 1. 1D electronic potential energy curves (CBS-QB3) for *cis*-HONO as functions of the central $r_{ON,c}$ bond length. The red arrow represents a vertical transition from the anion equilibrium geometry to the ground S_0 and excited T_1 states of neutral HONO. Note: *cis*-HONO (T_1) is unstable with respect to isomerization to *trans*-HONO (T_1), so what appears to be a minimum on the T_1 potential surface near 1.4 Å in this coordinate is actually a saddle point.

level of electronic structure was made based on the consistency between the results of the MP2 and CCSD(T) calculations, as is discussed in the Supporting Information. By use of the geometry, harmonic frequencies, and first-order anharmonicity constants from the MP2/aug-cc-pVTZ calculations, Franck–Condon factors (FCFs) were calculated for transitions from *cis*-$HONO^-$ to *cis*-HONO (S_0) using the PESCAL program.[35,36] When available, experimentally determined harmonic frequencies[14,37,38] and first-order anharmonicity constants[14] of *cis*-HONO (S_0) were used to determine the transition energies in the PESCAL simulation. When such information was not available, anharmonicity constants derived from the current experimental work (see Supporting Information) or calculated here (MP2/aug-cc-pVTZ) were used (see Table S3 for a summary of the values used in the PESCAL simulation). It is important that anharmonic corrections for the vibrational energies of *cis*-HONO (S_0) were used in this analysis because of the extended vibrational progression anticipated following electron photodetachment from *cis*-$HONO^-$. We do not expect significant population in excited vibrational levels of the anion because of the unique cooling capability of the ion source used in this experiment and, indeed, did not see evidence of this (as discussed below). Thus, the harmonic frequencies for the anion from the UMP2/aug-cc-pVTZ calculations were used in the FCF calculation. For comparison of the PESCAL calculated FCF stick spectrum with the experimental data, we convolute the FCFs with Gaussian functions. For each FCF, the Gaussian function is characterized by an area equal to the intensity of the calculated FCF and a fwhm dictated by its position (in eKE), in order to match our experimental resolution (fwhm/eKE) of approximately 3%.

To model electron photodetachment forming *cis*-HONO (T_1), calculations proceeded in two steps. First, a two-dimensional scan of the potential energy surface for *cis*-$HONO^-$ as a function of $r_{ON,c}$ and the terminal N═O bond length (labeled as $r_{NO,t}$ for the remainder of this manuscript) was performed using the CBS-QB3 composite method, as implemented in Gaussian 09.[34] For each point in the scan, $HONO^-$ was constrained to a planar *cis* configuration, and the energy was minimized with respect to the remaining three coordinates (OH bond length and HON and ONO angles). The potential was calculated for a grid ranging from 1.0 to 2.2 Å in $r_{NO,t}$ and from 1.2 to 3.0 Å in $r_{ON,c}$ in increments of 0.1 Å. Single-point energies for *cis*-HONO (T_1) were calculated at the *cis*-$HONO^-$ geometries from the *cis*-$HONO^-$ two-dimensional potential energy surface scan. The choice to evaluate the T_1 surface at the anion optimized geometries provided a better representation of the vertical transition region. It should be noted that at large values of $r_{ON,c}$ and $r_{NO,t}$, which correspond to high energy structures on the anion surface, the lowest energy geometry of $HONO^-$ does not correspond to the *cis* isomer. In these cases, the values of the HON and ONO angles, as well as the OH bond length, were constrained to their optimized values at the largest values of $r_{ON,c}$ and $r_{NO,t}$ for which *cis*-$HONO^-$ did not isomerize.

The anion and T_1 potential energy surfaces are used in the calculation of the photoelectron spectrum based on a two-dimensional model Hamiltonian:

$$H = \frac{1}{2\mu_{NO}}(p_{ON,c}^{\ 2} + p_{NO,t}^{\ 2}) + \frac{1}{2}\left(p_{ON,c}\frac{\cos\theta_{ONO}}{m_N}p_{NO,t} + p_{NO,t}\frac{\cos\theta_{ONO}}{m_N}p_{ON,c}\right) + V(r_{ON,c},r_{NO,t}) \quad (1)$$

where the value of the ONO angle depends on the two NO bond lengths. The calculation was performed using a discrete variable representation (DVR) for the two NO bond lengths.[39] For $r_{NO,t}$, 100 DVR points were used in the range of 1.0–2.2 Å, while 750 DVR points spanning 1.2–6.3 Å were used for $r_{ON,c}$. The calculated values of the *cis*-HONO (T_1) potential surface were extrapolated to values of $r_{ON,c}$ that extend beyond the range of calculated electronic energies by assuming an asymptotic form for the potential of

$$V_{asy} = V_\infty - \frac{C_6}{r_{ON,c}^{\ 6}} \quad (2)$$

and fitting the V_∞ and C_6 variables to the calculated values of the potential energy at $r_{ON,c}$ of 2.0 and 2.1 Å.

The calculation of the photoelectron spectrum was performed in two steps. In the first, for every value of $r_{ON,c}$, a one-dimensional calculation of the energies and wave functions for the $v = 0–3$ levels in $r_{NO,t}$ was performed, yielding terminal N═O stretch eigenfunctions. Then the two-dimensional Hamiltonian in eq 1 was solved in the product basis of sinc-DVR functions[39] in the central O–N stretch and these terminal N═O stretch eigenfunctions. The treatment of the kinetic coupling follows earlier work of Gardiner et al. on $H_4O_2^+$.[40,41] The resulting energies and wave functions were used to construct a photoelectron spectrum within the Franck–Condon approximation. This is shown and discussed further in section III.B.

III. RESULTS AND DISCUSSION

An overview photoelectron spectrum of *cis*-$HONO^-$ resulting from electron photodetachment using 3.49 eV photon energy is

DOI: 10.1021/acs.jpca.5b11797
J. Phys. Chem. A 2016, 120, 1652–1660

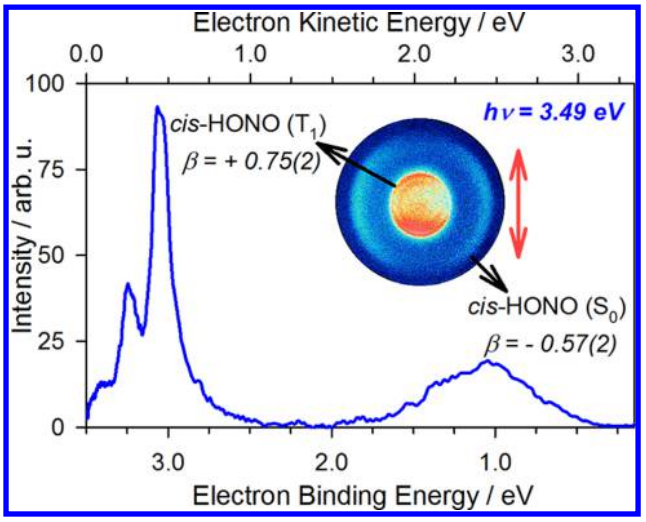

Figure 2. *cis*-HONO$^-$ photoelectron spectrum using 355 nm (3.49 eV) photons. The inset is the unprocessed velocity-mapped image of the photodetached electrons, illustrating the difference in electron angular distribution relative to the laser polarization (red double-headed arrow) following electron photodetachment forming the ground S_0 and excited T_1 states of *cis*-HONO.

shown in Figure 2. Two broad bands of peaks are clearly discernible in the raw image, as well as in the reconstructed photoelectron spectrum: a band at low eBE (high velocity, outer ring of the image) and another at high eBE (low velocity, inner rings of the image). The two bands arise from electron photodetachment forming different electronic states of *cis*-HONO. Other photodetachment wavelengths will permit investigation of these bands with much higher photoelectron energy resolution.

Neutral *cis*-HONO is a closed-shell singlet in its ground state (S_0) configuration.[7] The extra electron in *cis*-HONO$^-$ is added to the π^* antibonding orbital (3a″), which is localized along the central O−N bond. This electron may be removed in electron photodetachment, producing the S_0 state of *cis*-HONO. Alternatively, an electron could be removed from the next highest energy orbital, 10a′.[7] Removal of one of these electrons will result in either a singlet (S_1) or triplet (T_1) electronically excited state of *cis*-HONO. The electronic configurations corresponding to the observed experimental peaks in the photoelectron spectrum are identified through their relative energies and the photodetached electron angular anisotropy.

In Figure 2, the low eBE band (outer ring of image) extends from ∼0.3 eV to ∼2 eV electron binding energy, peaking near 1.1 eV. The photoelectron angular distribution of the low eBE band has a negative anisotropy parameter, with $\beta = -0.57(2)$, indicating photodetachment from a π-like molecular orbital. This result is consistent with the primarily π-like character of the calculated highest (singly) occupied molecular orbital of *cis*-HONO$^-$. The eBE and anisotropy of this band lead us to assign it to electron photodetachment of *cis*-HONO$^-$ forming the ground S_0 state of neutral *cis*-HONO.

The other band in the spectrum in Figure 2 starts near an eBE of 2.6 eV, approximately 2.3 eV higher in energy than the estimated origin of the low eBE band assigned to *cis*-HONO (S_0). The first excited singlet state (S_1) is experimentally known to be 3.26 eV higher in energy[23,24] than HONO (S_0) for the *cis* isomer. This would correspond to an eBE of over 3.5 eV, which is significantly higher in energy than the experimentally observed peaks starting near an eBE of 2.6 eV, and is inconsistent with this band corresponding to S_1. While there is no previous experimental information regarding the T_1 state of *cis*-HONO, calculations performed here (CBS-QB3 composite method) show an adiabatic excitation energy from S_0 to T_1 of approximately 2.58 eV for the *cis*-HONO isomer, in agreement with the observed approximate energy separation between the estimated origins of these two bands. Higher-level CASSCF/CASPT2 calculations were performed previously but only for *trans*-HONO.[7] In addition, the dominant peak in this band has a photoelectron angular distribution with $\beta = +0.75(2)$. The positive value of β indicates electron photodetachment from an orbital with more σ-like character than the lower eBE peak, consistent with detachment from the 10a′ second highest energy molecular orbital in *cis*-HONO$^-$. From the combination of the above attributes, we conclude that the band near eBE = 2.6 eV is likely from photodetachment to produce *cis*-HONO (T_1). These electronic state assignments will be validated with higher resolution spectra, vibrational analyses, and photoelectron spectrum simulations in the following two sections.

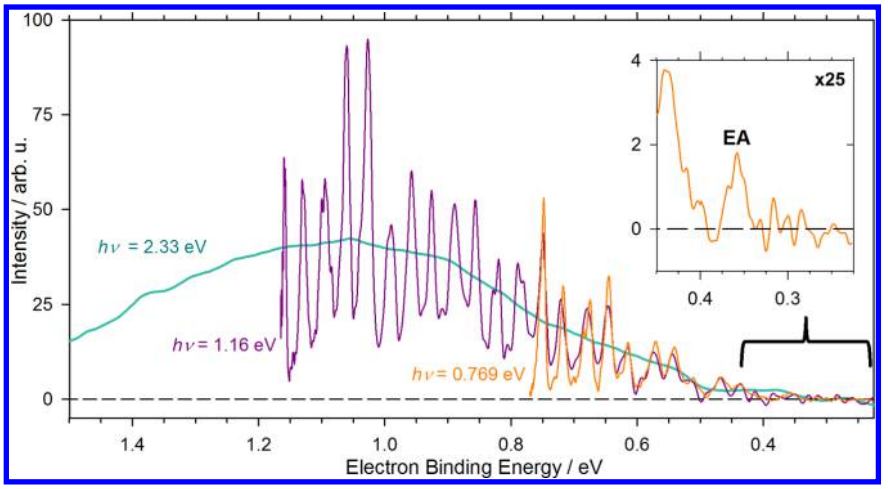

Figure 3. Photoelectron spectrum of *cis*-HONO$^-$ using photon energies of 532 nm (2.33 eV, green), 1064 nm (1.16 eV, purple), and 1613 nm (0.769 eV, orange). The change in resolution as a function of photon energy is characteristic of the VMI detection. The inset graphic shows a magnified view of the peak assigned as the EA.

DOI: 10.1021/acs.jpca.5b11797
J. Phys. Chem. A 2016, 120, 1652−1660

III.A. Ground State: *cis*-HONO $\tilde{X}\ ^1A'$. In this study, we take advantage of the changing resolution of the VMI detection with electron kinetic energy in order to obtain a better-resolved photoelectron spectrum by using lower energy photons to detach the electron from *cis*-$HONO^-$. The results of this process are illustrated in Figure 3 (the photoelectron spectrum scaling procedure is discussed in the Supporting Information). The 1.16 and 0.769 eV spectra, purple and orange traces of Figure 3, respectively, show well-resolved peaks and an improved signal-to-noise ratio. In contrast, the photoelectron spectrum using 2.33 eV photon energy mimics the band shown in Figure 2, showing a broad envelope with no discernible structure. Clearly, the broad photoelectron envelope observed when using photon energies well above the photodetachment threshold implies that the anion and neutral states involved have substantial structural differences and that both vibrational congestion and reduced electron energy resolution at these higher electron kinetic energies conspire to eliminate structure in the photoelectron spectrum.

Such spectral congestion could be anticipated, since there is a large change in geometry between the anion and neutral (S_0) *cis*-HONO structures based on quantum-chemical calculations performed here at the MP2/aug-cc-pVTZ level of theory/basis. There is a ~0.3 Å (~20%) decrease in $r_{ON,c}$ from the anion (1.657 Å) to the ground state neutral (1.387 Å) forms of *cis*-HONO. With the exception of the OH bond length (which decreases by 0.01 Å, or less than 0.5%), all of the other geometric parameters show ~4−10% increase in the bond lengths/decrease in the angles between the anion and neutral states (see Table S1). A common photoelectron signature of molecules with large changes in the geometry between the anion and neutral species is an almost uninterpretable photoelectron spectrum because of the spectral congestion. In some cases,[42,43] an experimental determination of the EA is very difficult because a large geometry change can result in an extremely weak origin transition compared to the most intense portions of the photoelectron spectrum.

The peak of the photoelectron spectrum reflects the photodetachment transition with the largest FCF, or the energy difference between the anion and neutral (S_0) electronic states of *cis*-HONO at the anion equilibrium geometry. This is referred to as the vertical detachment energy (VDE) and is ~1.1 eV for electron photodetachment to form *cis*-HONO (S_0). However, despite the nearly 0.8 eV energy difference between the VDE and the origin of the photoelectron spectrum, the lowest eBE peak at 0.358 eV is clearly visible above the signal-to-noise level when lower photon energies are used, as seen in the inset in Figure 3. There are no other peaks observed at lower eBE. This peak is labeled as peak A in Figure 4. In this figure, the concatenated photoelectron spectrum of *cis*-$HONO^-$ is plotted using the 1.16 eV spectrum for detachment energies above ~0.76 eV, and the 0.769 eV spectrum is plotted for smaller detachment energies. The resulting spectrum is shown as the black trace in Figure 4, where the major peaks in the experimental spectrum are alphabetically labeled. This concatenated spectrum has been corrected for the change in photodetachment cross section with electron kinetic energy, commonly referred to as the threshold effect,[44] which is further discussed in the Supporting Information. Peak A appears to be a single peak with, again, no observable peaks to lower eBE, while peaks B−C, D−F, and G−I show the start of a repeating pattern in the peak progression. We thus assign peak A as the origin transition; i.e.,

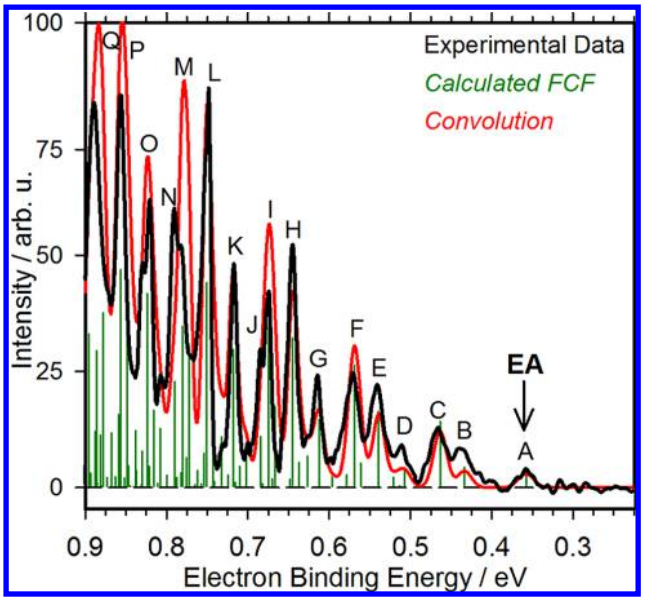

Figure 4. Scaled experimental photoelectron spectrum (black trace), Franck−Condon factors (green sticks), and convoluted simulation (red). The peak labels (upper case letters) refer to the *cis*-HONO $\tilde{X}\ ^1A'$ (S_0) vibrational assignments compiled in Table S2. For electron binding energies below ~0.76 eV, the black trace is identical to the 0.769 eV spectrum in Figure 3, while for large electron binding energies, the black trace reproduces the 1.16 eV spectrum shown in Figure 3.

the eBE for peak A is the EA(*cis*-HONO). This assignment is further supported by the photoelectron simulation, discussed below. It is important to recognize that the centers of these peaks will not necessarily correspond to the band origins of the transitions due to an asymmetry of the rotational band contour. By application of a small correction for this rotational shift,[45,46] the resulting EA(*cis*-HONO) is 0.356(8) eV (see Supporting Information). The calculated EA for *cis*-HONO is 0.324 eV, evaluated at the CCSD(T)/aug-cc-pVTZ level of theory, based on the optimized structures obtained using MP2/aug-cc-pVTZ (UMP2 for the anion, see Supporting Information). This value agrees very well with the experimental EA(*cis*-HONO). It is also consistent with the calculation performed here at a higher level of theory (CCSD(T)/aug-cc-pVTZ), resulting in EA(*cis*-HONO) = 0.352 eV.

The convolved and stick representations of the simulated spectrum (red trace and green sticks, respectively, in Figure 4) are used as an aid to assign the observed vibrational transitions of the dominant peaks in the experimental spectrum, the results of which are compiled in Table S6. The overall convolved photoelectron spectrum simulation shows excellent agreement with the experimental spectrum, despite the large degree of spectral congestion, particularly for eBE ≥ 0.7 eV. The peaks in the photoelectron spectrum are readily assigned, primarily to transitions to states involving excitation of overtones and combination bands of the central O−N stretch (ν_4) and the ONO bend (ν_5) along with states that have one quantum of excitation in the terminal N═O stretch (ν_2) and two fewer quanta of excitation in the central O−N stretch. This last set of states is attributed to the 2:1 Fermi resonance between ν_2 and $2\nu_4$. This progression in ν_4 is expected based on the geometry change between the anion and neutral forms of *cis*-HONO, discussed above. Further discussion of the vibrational assign-

DOI: 10.1021/acs.jpca.5b11797
J. Phys. Chem. A 2016, 120, 1652−1660

ments and derived spectroscopic constants is found in the Supporting Information.

The excellent agreement of the simulation with the experimental photoelectron spectrum provides support for the above peak assignments, particularly the EA, and the two assumptions that were made regarding the initially prepared *cis*-$HONO^-$: (1) the anion is vibrationally cold; (2) *cis*-$HONO^-$ is the dominant isomer present. First, there is no evidence for significant population in excited vibrational levels of *cis*-$HONO^-$, which would lead to vibrational hot bands in the photoelectron spectrum. The addition of hot bands into the photoelectron simulation greatly reduces its agreement with the experimental data. The absence of vibrational hot bands indicates that the anions are vibrationally cold, with vibrational temperatures below 150 K, typical of this ion source.[30] Second, the level of agreement between the experiment and simulation indicates that the *cis* isomer of $HONO^-$ is the dominant isomer formed in this experiment. The vibrational frequencies for *trans*-HONO are well-known experimentally[13,37] and are different from those for *cis*-HONO.[14,37] Thus, the experimental peak spacing in the spectrum is a good indication of which isomer is dominant, primarily in the low eBE (≤0.7 eV) range before the inclusion of anharmonicities and cross-anharmonicities become crucial to fitting the congested experimental spectrum. As shown in the Supporting Information, *trans*-$HONO^-$ cannot be the dominant isomer due to the poor agreement of the experimental peak spacings in the low eBE range of the spectrum with the experimentally known *trans*-HONO vibrational frequencies. While we cannot fully rule out the possibility that some *trans*-HONO is generated in the source, its contribution to the measured spectrum is small. This is supported by the observation that there are no experimentally observed peaks below 0.7 eV that remain unaccounted for when comparing the experimental spectrum with only the *cis*-$HONO^-$ photoelectron spectrum simulation. In other words, there is no experimental evidence that demands the inclusion of *trans*-$HONO^-$ in the analysis of the spectrum.

Potential energy surface scans of the torsional mode, i.e., isomerization from *cis*- to *trans*-$HONO^-$, were performed using the CBS-QB3 composite method, which indicate that the *cis* isomer is the lowest energy structure and is lower in energy than *trans*-$HONO^-$ by ∼0.03 eV. The barrier for isomerization from the *cis* to *trans* isomer is ∼0.05 eV (Figure S4). This differs from neutral HONO, where *trans* is the lowest energy isomer. Previous work with this ion source[30] on the association reaction $OH^- + CO \rightarrow HOCO^-$ showed evidence that both *cis*- and *trans*-$HOCO^-$ isomers were formed (vibrationally cold). The *cis*-$HOCO^-$ isomer is experimentally predicted to be more stable by 0.06 eV.[47] While the energy difference between this *cis* and *trans* isomers is similar for $HONO^-$ and $HOCO^-$, the isomerization barrier in $HOCO^-$, calculated using the CBS-QB3 composite method, is ∼0.4 eV, close to an order of magnitude larger than the corresponding barrier in $HONO^-$. The absence or significantly lower relative population of the *trans*-$HONO^-$ isomer could be due to the significantly lower barrier to isomerization: as $HONO^-$ is generated, the ions can more easily isomerize and be cooled to their global minimum before electron photodetachment rather than be trapped in a deep potential well as in the case of $HOCO^-$. A simple Boltzmann distribution of population indicates that there should be at most 13% *trans*-$HONO^-$ present at the rotational temperature of the spectrum (75 ± 25 K, see Supporting Information).

Table 1. Summary of the Experimentally Determined Quantities: Electron Affinity and Term Energies of *cis*-HONO and the Dissociation Energy of *cis*-$HONO^-$

parameter	experimental
electron affinity	0.356(8) eV
$D_0(HO^-–NO)$	0.594(9) eV
$\Delta E(T_1–S_0)$	∼2.3 eV

Since we do not see evidence for significant *trans*-$HONO^-$ population in the experiment, we expect this isomer to be higher in energy than *cis*-$HONO^-$, as predicted theoretically. We conclude, therefore, that *trans*-HONO has a smaller EA than the *cis* isomer, at least by 0.013(3) eV, which is the energy difference between the ground states of neutral *cis*- and *trans*-HONO,[22] i.e., EA(*trans*-HONO) ≤ 0.34 eV. The calculated EA for *trans*-HONO is 0.304 eV, evaluated at the CCSD(T)/aug-cc-pVTZ level of theory, based on the optimized structures obtained at the MP2/aug-cc-pVTZ level (ROMP2 for the anion). This is similar to the calculated EA(*trans*-HONO) = 0.289 eV, using CCSD(T)/aug-cc-pVTZ. An experimental measurement of the EA for *trans*-HONO has yet to be accomplished. In the reported photoelectron spectrum, if *trans*-$HONO^-$ is present, the peak for the EA(*trans*-HONO) must be at or below the noise level in the low eBE range of the spectrum ($\sigma_{noise} \approx 0.6$), which is at least 6.5 times smaller than "peak A", EA(*cis*-HONO). For further discussion of the relative contributions of the *cis* and *trans* isomers, see section B of the Supporting Information.

Using the experimentally measured EA(*cis*-HONO), we can also obtain the bond dissociation energy (D_0) for *cis*-$HONO^- \rightarrow OH^- + NO$, referred to here as $D_0(HO^-–NO)$, via the thermodynamic cycle,

$$D_0(HO^-–NO) = D_0(HO–NO) + EA(\textit{cis}\text{-HONO}) - EA(OH) \quad (3)$$

where $D_0(HO–NO) = 2.066(4)$ eV[16,22] and the EA(OH) = 1.828 eV.[48] This results in $D_0(HO^-–NO) = 0.594(9)$ eV, significantly improving an earlier calculated value of 0.49 eV (Gaussian 2 composite method).[17] These results are summarized in Table 1. As previously noted, the extra electron in *cis*-$HONO^-$ is added to a π^*-like antibonding molecular orbital, mainly localized along the central O–N bond. This results in a lengthening and weakening of the central bond upon the addition of an electron, consistent with the experimentally derived decrease in the O–N bond strength in *cis*-$HONO^-$ compared to neutral *cis*-HONO.

The very weak central bond of *cis*-$HONO^-$ and the small EA(*cis*-HONO) imply that it is unlikely that *cis*-$HONO^-$ would be able to be formed via the reaction of OH^- + NO and collisionally stabilized in the troposphere before falling apart or undergoing electron autodetachment.[17] However, if *cis*-$HONO^-$ is formed and stabilized, it would readily undergo photodetachment with any wavelength shorter than about 3000 nm. With a VDE of ∼1.1 eV, formation of neutral *cis*-HONO via photodetachment will preferentially be formed vibrationally hot, hence requiring less energy for dissociating and producing OH and NO radicals in the atmosphere.

III.B. Triplet State: *cis*-HONO $\tilde{a}\ ^3A''$. Figure 5 shows the 301 nm (4.12 eV) photoelectron spectrum of *cis*-$HONO^-$, spanning the T_1 excited state of *cis*-HONO. The excited state spectrum lies ∼2.3 eV higher in energy than *cis*-HONO (S_0)

DOI: 10.1021/acs.jpca.5b11797
J. Phys. Chem. A 2016, 120, 1652–1660

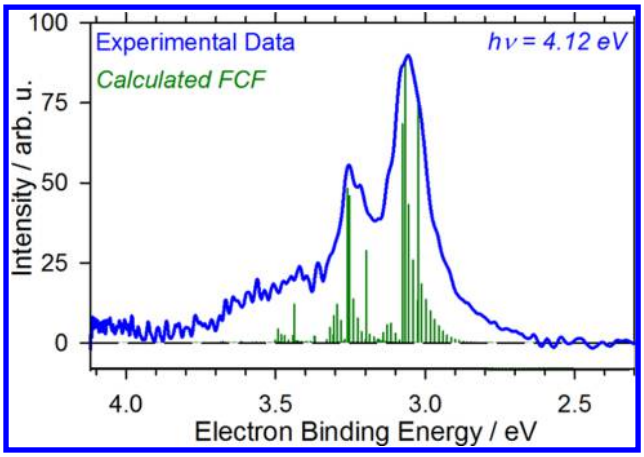

Figure 5. Detailed T_1 excited state photoelectron spectrum of *cis*-$HONO^-$ using 301 nm (4.12 eV) photon energy. The green sticks are the calculated FCFs by the methods described in the text.

and consists of three peaks that are an order of magnitude broader (0.09 eV fmwh at 3.1 eV eBE) than the resolution of the photoelectron spectrometer in this electron kinetic energy range. This result means that the breadth of these three peaks is intrinsic to the electron photodetachment and not due to our experimental resolution. The peaks in the spectrum are spaced by roughly 0.195 eV, or 1570 cm^{-1}. This energy is similar to the calculated frequency of the terminal N═O stretch in *cis*-HONO (T_1) (1414 cm^{-1}, CBS-QB3 composite method). A terminal N═O stretching vibration contribution to the photoelectron spectrum is also indicated based upon the calculated decrease in $r_{NO,t}$, from 1.25 to1.23 Å from the anion to neutral (T_1) equilibrium structures.

The potential energy curve for *cis*-HONO (T_1) at the equilibrium geometry of *cis*-$HONO^-$ exhibits a transition state along the $r_{ON,c}$ dissociation coordinate, as shown in Figure 1. In order to model the experimentally observed photoelectron spectrum, we calculate the FCFs (green sticks in Figure 5) by approximating the transitions as bound to bound, as outlined in section II.B. Essentially, an infinite potential wall is placed at large $r_{ON,c}$ distances on the T_1 potential energy curve, which allows for quantization of states along this HO−NO bond dissociation coordinate. While this is an approximation, the placement of an infinite wall only affects the density of states and not the overall shape of the envelope.

The overall shape of the calculated spectral envelope matches the experimental spectrum very well. The three main groups of peaks in the calculated spectrum reflect the active terminal N═O stretching vibration, as expected based on the experimental spacing of the peaks. Within each of these groups, there are two sets of peaks, which reflect the two regions of the T_1 surface that can be accessed by the ground state wave function of the anion. The anion wave function has significant amplitude over a large range of $r_{ON,c}$. When this wave function is projected onto the triplet surface, it samples both scattering and bound states in the O−N bond dissociation coordinate. The relative intensities of these two types of transitions are sensitive to details of the triplet potential surface. In order to approximately reproduce the experimental peak contour, the triplet surface was shifted to larger $r_{ON,c}$ distances by ∼0.08 Å relative to the anion surface. This shift is consistent with the variability of the calculated equilibrium $r_{ON,c}$ bond length for the anion at several levels of electronic structure theory (see Supporting Information). Due to the shallow anion potential energy surface along the central ON bond stretching coordinate, the $r_{ON,c}$ in the anion optimized geometry spans a range of 0.2 Å. The potential shift results in an increase in the contribution of transitions to states that are localized in the well on the T_1 state of *cis*-HONO to the overall band contour. In addition, the energy scale of the calculated FCFs was shifted by ∼30 meV to larger electron binding energy to more closely match the energetic position of the experimental spectrum. This shift roughly reflects the difference between the experimentally measured and calculated EA(*cis*-HONO).

The calculation indicates that the majority of the experimental peak breadth is due to the dissociation along $r_{ON,c}$, which would lead to the formation of OH and NO radicals. This analysis does not include other, smaller sources of peak broadening, such as rotational excitation of the separating OH and NO moieties, as well as activity in other *cis*-HONO (T_1) vibrations. However, out of the possible active vibrations based on the geometry differences between the anion and *cis*-HONO (T_1) equilibrium structures, only the N═O stretch remains bound following dissociation, and as such (unlike electron photodetachment to form the ground singlet state), only a progression in this vibration is expected to be reflected in the spectrum. Additional calculations show that including the torsion coordinate adds some further peak broadening but does not change the overall contour. While the triplet potential energy surface is plotted only along one coordinate in Figure 1, the local maximum in the blue curve is actually a second order saddle point, with the other imaginary frequency corresponding to the *cis*-HONO torsion. In other words, at the equilibrium geometry of *cis*-$HONO^-$, *cis*-HONO (T_1) is unstable with respect to isomerization to *trans*-HONO as well as to dissociation to OH + NO, and it is this feature of the T_1 state potential that is responsible for the broadening.

There could also be a contribution to the photoelectron spectrum shown in Figure 5 from photodetachment to *cis*-HONO (S_1). Now that there is an experimental measurement of the EA of *cis*-HONO (0.356(8) eV) and a known S_0−S_1 term energy (3.26 eV),[24] the expected onset of the photoelectron spectrum corresponding to *cis*-HONO (S_1) would be near 3.62 eV. The S_1 state of *cis*-HONO is known to be dissociative along the central HO−NO bond stretching coordinate,[7] and so it might also exhibit broadened peaks. Any contribution of the S_1 state to the photoelectron spectrum assigned to detachment to *cis*-HONO (T_1) is not conclusively identified, although there are photodetached electrons with very low kinetic energy seen in both the unprocessed photoelectron image (not shown) and the photoelectron spectrum (Figure 5). Higher energy photons could be used to explore detachment to *cis*-HONO (S_1); however, this state has been the focus of many past experimental studies[23,24] and current experimental details (particularly the large amount of background photoelectrons when using ultraviolet photon energies) inhibit this from being pursued further.

The major implication for the *cis*-HONO (T_1) analysis stems from its potential atmospheric relevance as a source of OH radicals. For the photodissociation of *cis*-HONO (S_0), producing OH radicals in the atmosphere, UV excitation accesses several higher lying singlet excited states. There is potential for intersystem crossing to play a role in the dissociation mechanism, as suggested by previous calculations.[7,27] The relative energies of the *cis*-HONO (T_1) and *cis*-HONO (S_0) electronic states (∼2.3 eV), as well as the

DOI: 10.1021/acs.jpca.5b11797
J. Phys. Chem. A 2016, 120, 1652−1660

dissociation to form OH + NO from the triplet surface, are instructive to future theoretical investigations.

IV. CONCLUSIONS

We report the experimental photoelectron spectrum of *cis*-$HONO^-$. In this experiment, *cis*-$HONO^-$ was formed in an association reaction of OH^- and NO in a pulsed plasma-entrainment ion source. We observe the presence of only the *cis*-$HONO^-$ isomer, which is calculated to be the global minimum on the anion potential energy surface. The reported photoelectron spectra show photodetachment to both the singlet ground state ($\tilde{X}\ ^1A'$) and the triplet state ($\tilde{a}\ ^3A''$) of neutral *cis*-HONO. On the basis of the photoelectron spectrum, we obtain the EA(*cis*-HONO) of 0.356(8) eV, with a VDE of approximately 1.1 eV. The large difference between the EA and the VDE is indicative of the significant geometry change upon electron photodetachment, which is consistent with the results of electronic structure calculations. In addition, detachment to form *cis*-HONO (S_0) exhibits a photoelectron spectrum dominated by excitation of the central O−N stretching vibration (ν_4), further confirming the significant change in $r_{ON,c}$ between the anion and neutral species. There are also significant contributions to the photoelectron spectrum from the ONO bending vibration (ν_5), particularly in combination bands with the central O−N stretching vibration. With the measurement of the EA, we also report the dissociation energy of the HO^-−NO bond as 0.594(9) eV. Electronic structure calculations and photoelectron spectra simulations reported here show excellent agreement with the experimental data, providing confidence in our vibrational assignments. The previously unobserved *cis*-HONO (T_1) state lies ∼2.3 eV higher in energy than *cis*-HONO (S_0). Vertical electron photodetachment from the anion onto the T_1 state potential energy surface accesses a transition state which results in dissociation to OH + NO, as well as an active bound N═O vibration. Table 1 summarizes these experimentally determined quantities. With this study, we provide new experimental data on *cis*-HONO and its lowest lying excited electronic state, as well as information about its negative ion *cis*-$HONO^-$. The information contained herein contributes to the knowledge of neutral *cis*-HONO as an important atmospheric species and precursor to OH radicals in the atmosphere.

■ ASSOCIATED CONTENT

Supporting Information

The Supporting Information is available free of charge on the ACS Publications website at DOI: 10.1021/acs.jpca.5b11797.

Additional information regarding experimental methods and analysis, experimental and calculated spectroscopic constants (PDF)

■ AUTHOR INFORMATION

Corresponding Authors

*A.B.M.: e-mail, abmccoy@uw.edu.

*W.C.L.: e-mail, wcl@jila.colorado.edu.

Notes

The authors declare no competing financial interest.

■ ACKNOWLEDGMENTS

W.C.L. gratefully acknowledges support from NSF (Grants PHY1125844 and CHE1213862) and AFOSR (Grant FA9550-12-1-0125) for significant contributions to this project. A.B.M. acknowledges financial support from the National Science Foundation (NSF Grants CHE-1213347 and CHE-1465001).

■ REFERENCES

(1) Indarto, A. Heterogeneous Reactions of HONO Formation From NO_2 and HNO_3: A Review. *Res. Chem. Intermed.* **2012**, *38*, 1029−1041.

(2) Kurtenbach, R.; Becker, K. H.; Gomes, J. A. G.; Kleffmann, J.; Lorzer, J. C.; Spittler, M.; Wiesen, P.; Ackermann, R.; Geyer, A.; Platt, U. Investigations of Emissions and Heterogeneous Formation of HONO in a Road Traffic Tunnel. *Atmos. Environ.* **2001**, *35*, 3385−3394.

(3) Kleffmann, J.; Gavriloaiei, T.; Hofzumahaus, A.; Holland, F.; Koppmann, R.; Rupp, L.; Schlosser, E.; Siese, M.; Wahner, A. Daytime Formation of Nitrous Acid: A Major Source of OH Radicals in a Forest. *Geophys. Res. Lett.* **2005**, *32*, L05818.

(4) Aubin, D. G.; Abbatt, J. P. D. Interaction of NO_2 with Hydrocarbon Soot: Focus on HONO Yield, Surface Modification, and Mechanism. *J. Phys. Chem. A* **2007**, *111*, 6263−6273.

(5) Finlayson-Pitts, B. J.; Pitts, J. N. *Chemistry of the Upper and Lower Atmosphere: Theory, Experiments, and Applications*; Academic Press: San Diego, CA, 2000.

(6) Asatryan, R.; Bozzelli, J. W.; Simmie, J. M. Thermochemistry for Enthalpies and Reaction Paths of Nitrous Acid Isomers. *Int. J. Chem. Kinet.* **2007**, *39*, 378−398.

(7) Yu, S. Y.; Zhang, C. G.; Huang, M. B. A CAS Study of the S_0, T_1, S_1, T_2, and S_2 States of the *trans*-HONO Molecule. *Chem. Phys. Lett.* **2007**, *440*, 187−193.

(8) Sengupta, D.; Sumathi, R.; Peyerimhoff, S. D. Unimolecular Decomposition of the Isomers of $[HNO_2]^+$ and $[HNO_2]^-$ Systems: A DFT Study. *Chem. Phys.* **1999**, *248*, 147−159.

(9) Spataro, F.; Ianniello, A. Sources of Atmospheric Nitrous Acid: State of the Science, Current Research Needs, and Future Prospects. *J. Air Waste Manage. Assoc.* **2014**, *64*, 1232−1250.

(10) VandenBoer, T. C.; Young, C. J.; Talukdar, R. K.; Markovic, M. Z.; Brown, S. S.; Roberts, J. M.; Murphy, J. G. Nocturnal Loss and Daytime Source of Nitrous Acid Through Reactive Uptake and Displacement. *Nat. Geosci.* **2015**, *8*, 55−60.

(11) Alicke, B.; Platt, U.; Stutz, J. Impact of Nitrous Acid Photolysis on the Total Hydroxyl Radical Budget During the Limitation of Oxidant Production/Pianura Padana Produzione Di Ozono Study in Milan. *J. Geophys. Res.* **2002**, *107*, LOP 9-1.

(12) Bartolomei, V.; Sorgel, M.; Gligorovski, S.; Alvarez, E. G.; Gandolfo, A.; Strekowski, R.; Quivet, E.; Held, A.; Zetzsch, C.; Wortham, H. Formation of Indoor Nitrous Acid (HONO) by Light-Induced NO_2 Heterogeneous Reactions with White Wall Paint. *Environ. Sci. Pollut. Res.* **2014**, *21*, 9259−9269.

(13) Guilmot, J. M.; Godefroid, M.; Herman, M. Rovibrational Parameters for *trans*-Nitrous Acid. *J. Mol. Spectrosc.* **1993**, *160*, 387−400.

(14) Guilmot, J. M.; Melen, F.; Herman, M. Rovibrational Parameters for *cis*-Nitrous Acid. *J. Mol. Spectrosc.* **1993**, *160*, 401−410.

(15) Reiche, F.; Abel, B.; Beck, R. D.; Rizzo, T. R. Double-Resonance Overtone Photofragment Spectroscopy of *trans*-HONO. II. State- And Time-Resolved Dissociation and OH-Product State Distributions. *J. Chem. Phys.* **2002**, *116*, 10267−10276.

(16) Reiche, F.; Abel, B.; Beck, R. D.; Rizzo, T. R. Double-Resonance Overtone Photofragment Spectroscopy of *trans*-HONO. I. Spectroscopy and Intramolecular Dynamics. *J. Chem. Phys.* **2000**, *112*, 8885−8898.

(17) Vandoren, J. M.; Viggiano, A. A.; Morris, R. A.; Miller, A. E. S.; Miller, T. M.; Paulson, J. F.; Deakyne, C. A.; Michels, H. H.; Montgomery, J. A. Experimental and Theoretical-Study of the Reaction of HO^- with NO. *J. Chem. Phys.* **1993**, *98*, 7940−7950.

(18) Finnigan, D. J.; Smith, J. G.; Cox, A. P.; Brittain, A. H. Centrifugal Distortion in Microwave-Spectra of *cis*-Nitrous and *trans*-Nitrous Acids - Determination of Quadratic Potential Functions and Average Structures. *J. Chem. Soc., Faraday Trans. 2* **1972**, *68*, 548−565.

DOI: 10.1021/acs.jpca.5b11797
J. Phys. Chem. A 2016, 120, 1652−1660

(19) Hall, R. T.; Pimentel, G. C. Isomerization of Nitrous Acid - an Infrared Photochemical Reaction. *J. Chem. Phys.* **1963**, *38*, 1889.
(20) Botan, V.; Hamm, P. Intramolecular Vibrational Energy Relaxation in Nitrous Acid (HONO). *J. Chem. Phys.* **2008**, *129*, 164506.
(21) Cox, A. P.; Brittain, A. H.; Finnigan, D. J. Microwave Spectrum, Structure, Dipole Moment and Quadrupole Coupling Constants of *cis* and *trans* Nitrous Acids. *Trans. Faraday Soc.* **1971**, *67*, 2179−2194.
(22) Sironneau, V.; Flaud, J. M.; Orphal, J.; Kleiner, I.; Chelin, P. Absolute Line Intensities of HONO and DONO in the Far-Infrared and Re-Determination of the Energy Difference Between the *trans*- and *cis*- Species of Nitrous Acid. *J. Mol. Spectrosc.* **2010**, *259*, 100−104.
(23) Bongartz, A.; Kames, J.; Welter, F.; Schurath, U. Near-UV Absorption Cross-sections and *trans-cis* Equilibrium of Nitrous-Acid. *J. Phys. Chem.* **1991**, *95*, 1076−1082.
(24) King, G. W.; Moule, D. Ultraviolet Absorption Spectrum of Nitrous Acid in the Vapor State. *Can. J. Chem.* **1962**, *40*, 2057−2065.
(25) Vasudev, R.; Zare, R. N.; Dixon, R. N. Dynamics of Photo-Dissociation of HONO at 369 nm - Motional Anisotropy and Internal State Distribution of the OH Fragment. *Chem. Phys. Lett.* **1983**, *96*, 399−402.
(26) Amaral, G.; Xu, K. S.; Zhang, J. S. H+NO_2 Channels in the Photodissociation of HONO at 193.3 nm. *J. Phys. Chem. A* **2001**, *105*, 1465−1475.
(27) Larrieu, C.; Dargelos, A.; Chaillet, M. Theoretical-Study of Nitrous-Acid Electronic-Spectrum and Photofragmentation. *Chem. Phys. Lett.* **1982**, *91*, 465−472.
(28) Shuman, N. S.; Hunton, D. E.; Viggiano, A. A. Ambient and Modified Atmospheric Ion Chemistry: From Top to Bottom. *Chem. Rev.* **2015**, *115*, 4542−4570.
(29) Sheps, L.; Miller, E. M.; Lineberger, W. C. Photoelectron Spectroscopy of Small $IBr^-(CO_2)_n$, (n=0-3) Cluster Anions. *J. Chem. Phys.* **2009**, *131*, 064304.
(30) Lu, Y. J.; Lehman, J. H.; Lineberger, W. C. A Versatile, Pulsed Anion Source Utilizing Plasma-Entrainment: Characterization and Applications. *J. Chem. Phys.* **2015**, *142*, 044201.
(31) Dribinski, V.; Ossadtchi, A.; Mandelshtam, V. A.; Reisler, H. Reconstruction of Abel-Transformable Images: The Gaussian Basis-Set Expansion Abel Transform Method. *Rev. Sci. Instrum.* **2002**, *73*, 2634−2642.
(32) Ervin, K. M.; Anusiewicz, W.; Skurski, P.; Simons, J.; Lineberger, W. C. The Only Stable State of O_2^- is the X ^2P_g Ground State and it (Still!) has an Adiabatic Electron Detachment Energy of 0.45 eV. *J. Phys. Chem. A* **2003**, *107*, 8521−8529.
(33) Hanstorp, D.; Gustafsson, M. Determination of the Electron-Affinity of Iodine. *J. Phys. B: At., Mol. Opt. Phys.* **1992**, *25*, 1773−1783.
(34) Frisch, M. J.; Trucks, G. W.; Schlegel, H. B.; Scuseria, G. E.; Robb, M. A.; Cheeseman, J. R.; Scalmani, G.; Barone, V.; Mennucci, B.; Petersson, G. A.; et al.; Gaussian, Inc.: Wallingford, CT, U.S., 2009.
(35) Ervin, K. M.; Ramond, T. M.; Davico, G. E.; Schwartz, R. L.; Casey, S. M.; Lineberger, W. C. Naphthyl Radical: Negative Ion Photoelectron Spectroscopy, Franck-Condon Simulation, and Thermochemistry. *J. Phys. Chem. A* **2001**, *105*, 10822−10831.
(36) Ervin, K. M.; Ho, J.; Lineberger, W. C. Ultraviolet Photoelectron-Spectrum of NO_2^-. *J. Phys. Chem.* **1988**, *92*, 5405−5412.
(37) Deeley, C. M.; Mills, I. M. The Infrared Vibration-Rotation Spectrum of *trans*-Nitrous and *cis*-Nitrous Acid. *J. Mol. Struct.* **1983**, *100*, 199−213.
(38) Khriachtchev, L.; Lundell, J.; Isoniemi, E.; Rasanen, M. HONO in Solid Kr: Site-Selective *trans* <-> *cis* Isomerization with Narrow-Band Infrared Radiation. *J. Chem. Phys.* **2000**, *113*, 4265−4273.
(39) Colbert, D. T.; Miller, W. H. A Novel Discrete Variable Representation for Quantum-Mechanical Reactive Scattering via the S-Matrix Kohn Method. *J. Chem. Phys.* **1992**, *96*, 1982−1991.
(40) Gardenier, G. H.; Johnson, M. A.; McCoy, A. B. Spectroscopic Study of the Ion-Radical H-Bond in $H_4O_2^+$. *J. Phys. Chem. A* **2009**, *113*, 4772−4779.
(41) Gardenier, G. H.; Johnson, M. A.; McCoy, A. B. Correction to "Spectroscopic Study of the Ion-Radical H-Bond in $H_4O_2^+$". *J. Phys. Chem. A* **2012**, *116*, 8797−8797.
(42) Bopp, J. C.; Roscioli, J. R.; Johnson, M. A.; Miller, T. M.; Viggiano, A. A.; Villano, S. M.; Wren, S. W.; Lineberger, W. C. Spectroscopic Characterization of the Isolated SF_6^- And $C_4F_8^-$ Anions: Observation of Very Long Harmonic Progressions in Symmetric Deformation Modes Upon Photodetachment. *J. Phys. Chem. A* **2007**, *111*, 1214−1221.
(43) Osborn, D. L.; Vogelhuber, K. M.; Wren, S. W.; Miller, E. M.; Lu, Y. J.; Case, A. S.; Sheps, L.; McMahon, R. J.; Stanton, J. F.; Harding, L. B.; et al. Electronic States of the Quasilinear Molecule Propargylene (HCCCH) from Negative Ion Photoelectron Spectroscopy. *J. Am. Chem. Soc.* **2014**, *136*, 10361−10372.
(44) Wigner, E. P. On the Behavior of Cross Sections Near Thresholds. *Phys. Rev.* **1948**, *73*, 1002−1009.
(45) Travers, M. J.; Cowles, D. C.; Clifford, E. P.; Ellison, G. B.; Engelking, P. C. Photoelectron Spectroscopy of the CH_3N^- ion. *J. Chem. Phys.* **1999**, *111*, 5349−5360.
(46) Engelking, P. C. Approximate Rotational Band Shifts. *J. Phys. Chem.* **1986**, *90*, 4544−4545.
(47) Johnson, C. J.; Harding, M. E.; Poad, B. L. J.; Stanton, J. F.; Continetti, R. E. Electron Affinities, Well Depths, and Vibrational Spectroscopy of *cis*- and *trans*-HOCO. *J. Am. Chem. Soc.* **2011**, *133*, 19606−19609.
(48) Smith, J. R.; Kim, J. B.; Lineberger, W. C. High-Resolution Threshold Photodetachment Spectroscopy of OH^-. *Phys. Rev. A: At., Mol., Opt. Phys.* **1997**, *55*, 2036−2043.

DOI: 10.1021/acs.jpca.5b11797
J. Phys. Chem. A 2016, 120, 1652−1660